$P < 0.05$, respectively). These increases were significantly inhibited in the diet/ESE group ($P < 0.05$ and $P < 0.05$, respectively).

Effect of ESE on diet-related fatty liver

H&E stained liver sections are shown in Figure 1. The normal group showed normal hepatic histology. The diet group showed characteristics of NASH, namely macrovesicular steatosis and hepatocellular ballooning. Slight fat deposition was seen in the diet/ESE group.

Effect of ESE on oxidative stress in liver tissue

Activities of SOD, GPx and catalase and levels of GSH and LPO in liver tissue are shown in Table 2. SOD, GPx and catalase activities were significantly lower in the diet group than in the normal group ($P < 0.05$, $P < 0.01$ and $P < 0.01$, respectively). SOD and GPx activities were significantly higher in the diet/ESE group than in the diet group ($P < 0.05$ and $P < 0.05$, respectively). There was no marked difference in catalase activity between the two groups.

The level of GSH in the liver tissue was significantly lower in the diet group than in the normal group ($P < 0.05$) but was significantly higher in the diet/ESE group than in the diet group ($P < 0.05$). The level of LPO in liver tissue was significantly higher in the diet group than in the normal group ($P < 0.01$) but was significantly lower in the diet/ESE than in the diet group ($P < 0.01$).

Effect of ESE on 8-OHdG and 4-HNE expression

Immunohistochemical staining of liver tissue is shown in Figure 2. Immunohistochemical staining of 8-OHdG (Figure 2a) is used as an index of oxidative DNA damage; 4-HNE (Figure 2b) is a secondary oxidation product of high-level unsaturated fatty acids. Neither 8-OHdG nor 4-HNE was detected in the normal group. Both 8-OHdG and 4-HNE were detected in the diet group but expression of both was inhibited in the diet/ESE group.

Effect of ESE on the liver levels of TGF-β

The level of TGF-β in liver tissue is shown in Figure 3a. Levels of TGF-β were significantly higher in the diet group than in the normal group (91.5 ± 15.0 vs 32.6 ± 11.2 pg/mg protein). Levels in the diet/ESE group (34.5 ± 9.0 pg/mg protein) were significantly lower than in the diet group. There was no significant difference between the diet/ESE and normal groups.

Effect of ESE on liver fibrosis

The level of collagen in liver tissue is shown in Figure 3b. The level in the diet group was significantly higher than in the normal group (33.7 ± 4.5 vs 18.4 ± 1.7 μg collagen/mg protein). The level in the diet/ESE group (23.5 ± 1.4 μg collagen/mg protein) was significantly lower than in the diet group. There was no significant difference between the diet/ESE and normal groups.

The results of Azan staining are shown in Figure 4. The normal group showed normal hepatic histology. The diet group showed the perivenular/pericellular fibrosis that is a heterogeneous pattern of fibrosis in NASH. Slight fibrosis was seen in the diet/ESE group.

Discussion

High levels of enzymes that mop up cellular oxygen, such as SOD, GPx and catalase, are present *in vivo*. However, when the production of ROS exceeds the capacity of these enzymes, oxidative stress induces various cellular responses[20] and may also play an important role in the onset and deterioration of NASH. A study reported that, in the presence of NASH, mitochondria in hepatocytes have morphological abnormalities that are involved in the excess production of ROS.[6]

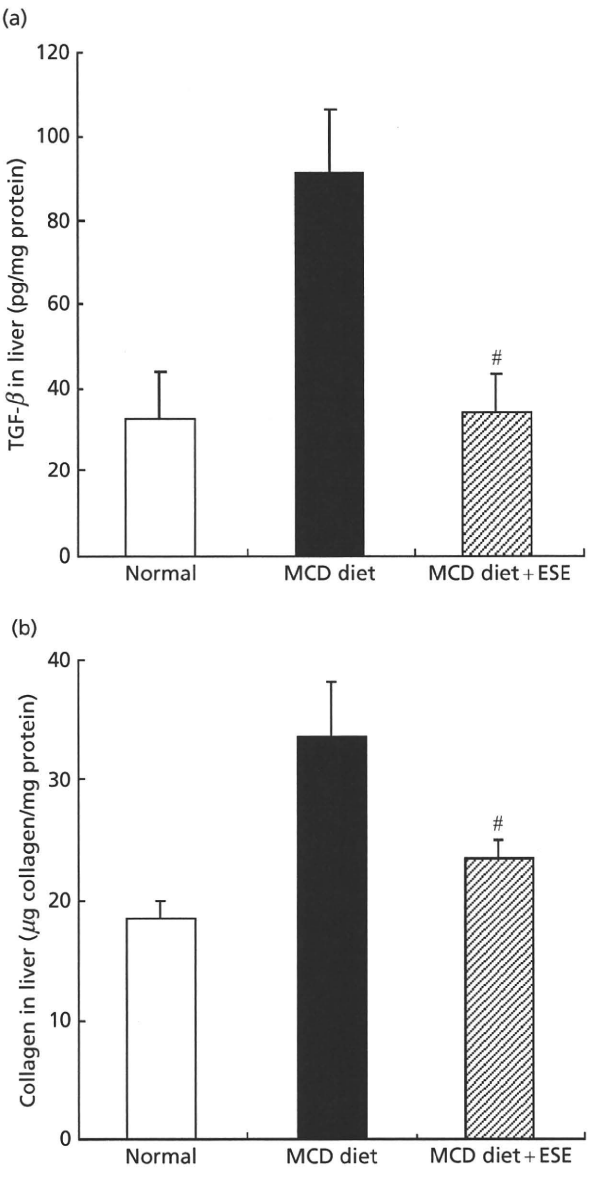

Figure 3 Effect of *E. japonica* seed extract (ESE) on liver tissue levels of (a) transforming growth factor-β (TGF-β) and (b) collagen. The significant increases in TGF-β and collagen induced by the methionine-choline-deficient (MCD) diet were reduced by concomitant treatment with ESE. Columns represent means ± SEM (n = 4–7 experiments). $^{*}P < 0.05$; $^{**}P < 0.01$ vs normal group; $^{\#}P < 0.05$ vs MCD diet group (Tukey–Kramer's test).

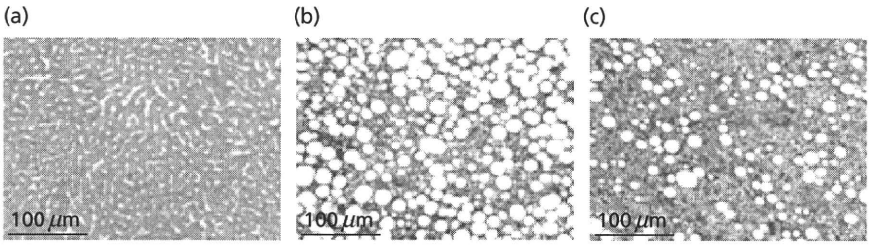

Figure 4 Effect of *E. japonica* seed extract (ESE) on liver fibrosis, demonstrated by Azan staining. Representative liver samples from rats fed (a) a normal diet, (b) a methionine-choline-deficient (MCD) diet or (c) the MCD diet with ESE in the drinking water. Collagen fibres are stained blue in the photomicrographs.

Furthermore, an excess level of fatty acids in the liver enhances mitochondrial β-oxidation, leading to oxidative stress via the excess production of CYP2E1.[21] In addition, various factors such as an excess amount of iron ions may be involved.[22,23]

In this study, we used rats fed an MCD diet as a NASH model. Decreases in the liver levels of methionine and choline promote the excess production of ROS, inducing oxidative stress and leading to hepatocellular disorder and adipose cell formation. In addition, choline deficiency affects lipid metabolism, resulting in fatty liver.[24]

We have investigated ESE because of its antioxidant actions.[14–17] In addition, the usefulness of ESE administration has also been suggested in a hyperlipidaemia model.[19]

ESE administration inhibited increases in the AST and ALT levels, preventing the onset of hepatitis. H&E staining confirmed the inhibitory effects of ESE on fat deposition in the liver. This was possibly associated with the cholesterol-reducing actions of ESE previously reported.[19] With respect to the effects of ESE on oxidative stress, ESE administration increased SOD and GPx activities and reduced oxidative stress by increasing the level of GSH (an antioxidant substance), and decreasing the LPO level. A previous study reported the hydroxyl radical and superoxide anion scavenging actions of ESE.[13]

Oxidative stress may be enhanced in the presence of a fatty liver, leading to the appearance of various types of ROS, suggesting that it can induce excessive DNA/lipid oxidation in the liver. ESE, with its antioxidant actions, inhibited the nuclear expression of 8-OHdG and intracellular expression of 4-HNE, suggesting that it reduces excessive DNA/lipid oxidation in the liver. LPO, which is generated in the presence of oxidative stress, may contribute to the progression of liver fibrosis by activating Kupffer cells, which produce collagen, and promoting the production of cytokines such as TGF-β. In our NASH model, levels of TGF-β and collagen were decreased in rats treated with ESE, suggesting that ESE has potent antioxidant actions. Azan staining confirmed the inhibitory effects of ESE administration on liver fibrosis.

Declarations

Conflict of interest

The Author(s) declare(s) that they have no conflicts of interest to disclose.

Funding

This research/review received no specific grant from any funding agency in the public, commercial or not-for-profit sectors.

References

1. Ludwig J *et al.* Nonalcoholic steatohepatitis: Mayo Clinic experiences with a hitherto unnamed disease. *Mayo Clin Proc* 1980; 55: 434–438.
2. Younossi ZM *et al.* Nonalcoholic fatty liver disease: an agenda for clinical research. *Hepatology* 2002; 35: 746–752.
3. Kojima S *et al.* Increase in the prevalence of fatty liver in Japan over the past 12 years: analysis of clinical background. *J Gastroenterol* 2003; 38: 954–961.
4. Farrell GC. Non-alcoholic steatohepatitis: what is it, and why is it important in the Asia-Pacific region? *J Gastroenterol Hepatol* 2003; 18: 124–138.
5. Day CP, James OFW. Steatohepatitis: a tale of two "hits"? *Gastroenterology* 1998; 114: 842–845.
6. Le TH *et al.* The zonal distribution of megamitochondria with crystalline inclusions in nonalcoholic steatohepatitis. *Hepatology* 2004; 39: 1423–1429.
7. Suzuki D *et al.* Liver failure caused by non-alcoholic steatohepatitis in an obese young male. *J Gastroenterol Hepatol* 2005; 20: 327–329.
8. Marchesini G *et al.* Metformin in non-alcoholic steatohepatitis. *Lancet* 2001; 358: 893–894.
9. Laurin J *et al.* Ursodeoxycholic acid or clofibrate in the treatment of non-alcohol-induced steatohepatitis: a pilot study. *Hepatology* 1996; 23: 1464–1467.
10. Saibara T *et al.* Bezafibrate for tamoxifen-induced non-alcoholic steatohepatitis. *Lancet* 1999; 353: 1802.
11. Yokohama S *et al.* Therapeutic efficacy of an angiotensin II receptor antagonist in patients with nonalcoholic steatohepatitis. *Hepatology* 2004; 40: 1222–1225.
12. Hirose A *et al.* Angiotensin II type 1 receptor blocker inhibits fibrosis in rat nonalcoholic steatohepatitis. *Hepatology* 2007; 45: 1375–1381.
13. Yokota J *et al.* Scavenging of reactive oxygen species by *Eriobotrya japonica* seed extract. *Biol Pharm Bull* 2006; 29: 467–471.
14. Takuma D *et al.* Effect of *Eriobotrya japonica* seed extract on 5-fluorouracil-induced mucositis in hamsters. *Biol Pharm Bull* 2008; 31: 250–254.
15. Yokota J *et al.* Gastroprotective activity of *Eriobotrya japonica* seed extract on experimentally induced gastric lesions in rats. *J Nat Med* 2008; 62: 96–100.

16. Hamada A *et al.* The effect of *Eriobotrya japonica* seed extract on oxidative stress in adriamycin-induced nephropathy in rats. *Biol Pharm Bull* 2004; 27: 1961–1964.
17. Sun G *et al.* Effect of orally administered *Eriobotrya japonica* seed extract on allergic contact dermatitis in rats. *J Pharm Pharmacol* 2007; 59: 1405–1412.
18. Onogawa M *et al.* Animal studies supporting the inhibition of mast cell activation by *Eriobotrya japonica* seed extract. *J Pharm Pharmacol* 2009; 61: 237–241.
19. Nishioka Y. Medicine composition that contains *Eriobotrya japonica* seed extract to adjust amount of lipid in body fluids. 2003; JP 3438029.
20. Sies H. Oxidative stress: from basic research to clinical application. *Am J Med* 1991; 91: 31S–38S.
21. Chalasani N *et al.* Hepatic cytochrome P450 2E1 activity in nondiabetic patients with nonalcoholic steatohepatitis. *Hepatology* 2003; 37: 544–550.
22. Valenti L *et al.* Alpha 1-antitrypsin mutations in NAFLD: high prevalence and association with altered iron metabolism but not with liver damage. *Hepatology* 2006; 44: 857–864.
23. Nelson JE *et al.* HFE C282Y mutations are associated with advanced hepatic fibrosis in Caucasians with nonalcoholic steatohepatitis. *Hepatology* 2007; 46: 723–729.
24. Takei Y *et al.* Choline deficiency and NAFLD. In: Saibara T, ed. *Nonalcoholic Fatty Liver Disease: NAFLD – from the base to clinic.* Tokyo: Ishiyaku Publishers Inc, 2006: 159–162.

Int J Clin Exp Pathol 2010;3(6):634-639
www.ijcep.com /IJCEP1005007

Case Report

Matrix metalloproteinase-1 expression in splenic angiosarcoma metastasizing to the serous membrane

Tamotsu Takeuchi[1], Shinji Iwasaki[2], Junichi Miyazaki[3], Yasuko Nozaki[2], Masaya Takahashi[2] , Masafumi Ono[2], Toshiji Saibara[2], Mutsuo Furihata[1]

[1]Department of Pathology, [2]Department of Gastroenterology and Hepatology, Kochi Medical School, Nankoku, Japan 783-8505, and [3]Department of Clinical Pathology, Kochi Prefectural Hata Kenmin Hospital, Kochi 788-0785, Japan

Received May 26, 2010, accepted June 9, 2010, available online June 25, 2010

Abstract: Angiosarcoma involving the serous membrane may mimic mesothelioma; therefore, the term "pseudomesotheliomatous angiosarcoma" has been suggested for this entity. However, the pathogenesis of pseudomesotheliomatous angiosarcoma remains unclear. Here, we report an autopsy case of splenic angiosarcoma, which systemically metastasized to the serous membrane of both the peritoneum and pleura, closely resembling a mesothelioma. The spindle-shaped tumor cells exhibited marked invasion of the lymphatic vessels and invaded the serous membrane causing thickening of the fibrous tissues like desmoplastic mesothelioma. In the present case, immunohistochemical staining showed that the tumor expressed not only the endothelial cell markers, such as CD31, vascular endothelial growth factor receptor 3, and podoplanin (D2-40), but also matrix metalloproteinase-1 (also known as collagenase-1), which is known to increase the invasiveness of mesothelioma cells. MMP-1 expression was not observed in the other cases of angiosarcoma, examined. This tumor might systemically metastasize to the serous membrane via the lymphatic route and might generate the fibrous stroma aided by the matrix metalloproteinase-1.

Keywords: Angiosarcoma, pseudomesothelioma, MMP-1, collagenase-1

Introduction

Angiosarcoma is characterized by aggressive biological behavior and high metastatic rate [1]. Splenic angiosarcoma is highly metastatic, often metastasizing to the liver, lung, and bones through hematogenous dissemination and rarely to the regional lymph nodes [2]. However, the metastasis of splenic angiosarcoma to the serous membrane is quite uncommon.

Angiosarcoma involving the serous membrane could mimic mesothelioma; thus, the term "pseudomesotheliomatous angiosarcoma" has been suggested for this entity [3-5]. Pseudomesotheliomatous angiosarcoma is rare; therefore, its pathogenesis remains largely unclear. In addition, the location of the primary lesion of pseudomesotheliomatous or serosal angiosarcoma is sometimes unclear because multiple tumor sites, i.e., liver and/or lung, have been found to be involved at the time of diagnosis [4].

Some investigators have speculated that serosal angiosarcoma could represent a peculiar malignant mesothelioma differentiating along an abnormal angioblastic pathway [6]. However, others think that most pseudomesotheliomatous angiosarcomas originate near a serosal surface and rapidly spread over the serous membrane, thereby masking their origin [7].

Here, we report a case of splenic angiosarcoma, which exhibited an unusual metastasis to the peritoneum and pleura, closely resembling a mesothelioma. This tumor exhibited marked invasion of the lymphatic vessels in the peritoneum and pleura. Notably, the present angiosarcoma cells expressed matrix metalloproteinase-1 (MMP-1; also known as collagenase-1) that is also expressed by many mesothelioma cells. However, we could not detect MMP-1 expression in the other examined angiosarcoma cells, which did not show metastasis to the serous membrane. Recent studies have highlighted that MMP-1 may play a critical role in the

development of mesothelioma [8-10]. We think that both invasion to the lymphatic vessels and MMP-1 expression might be related to the peculiar metastatic pattern of the studied angiosarcoma cells.

Case history

The patient was a 37-year-old, previously healthy male, who presented with low back pain and abdominal bloating. He had no history occupational exposure to asbestos. On the basis of the clinical examination, including computerized tomography (CT), the patient was suspected to have splenomegaly and underwent splenectomy. Splenectomy specimen was 18×16×13 cm in size and weighted 1800g and was diagnosed with primary splenic angiosarcoma after the final pathological examination. At the time of splenectomy, any unusual serous change was observed by CT or even by direct observation of the peritoneum.

A year after splenectomy, the patient had massive ascites and pleural effusion with peritoneal and pleural wall thickening (**Figure 1**). The patient underwent radiotherapy (45 Gy and 56 Gy to the abdomen and chest, respectively, for a year), but his condition deteriorated, and he died 2 years after splenectomy. After obtaining the consent of the patient's family, an autopsy was performed 1hr after death.

Autopsy examination

At the time of the autopsy, the peritoneum and pleura—both parietal and visceral—showed marked thickening, thereby mimicking a mesothelioma. Moreover, the mesentery was also thickened by marked fibrosis. The angiosarcoma also metastasized to the liver, bone marrow, and systemic lymph nodes.

The representative histopathological findings including that of primary splenic focus are shown in **Figure 2**. The spindle-shaped tumor cells diffusely expanded along the serous membrane with densely collagenized stroma, thereby mimicking the desmoplastic mesothelioma. Lymphatic invasion was frequently found in both the peritoneum and pleura. Notably, some tumor cells exhibited rudimentary slit-like vascular spaces (**Figure 2D**). The tumor cells also expanded along the sinusoid space in the liver. In addition, the tumor cells exhibited focal growth with the fibrous tissues in the bone marrow.

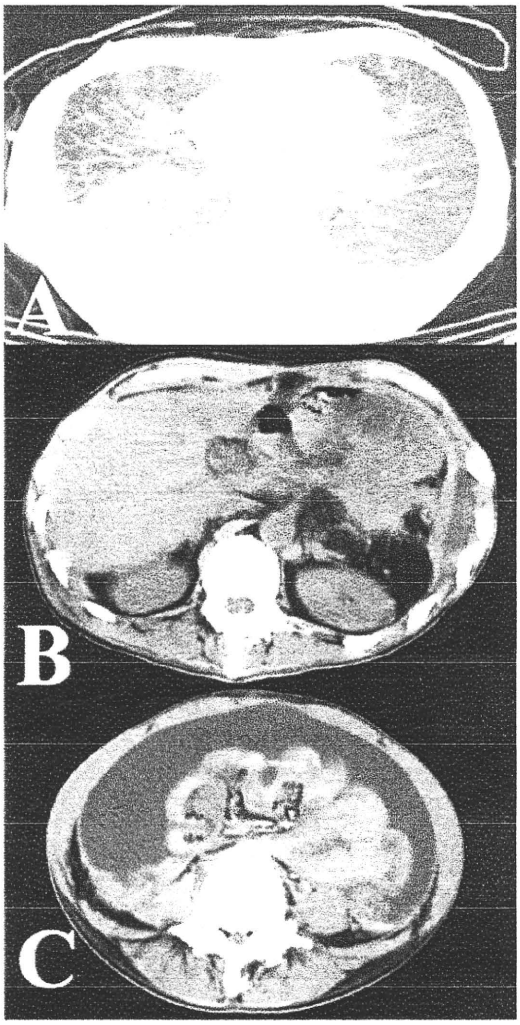

Figure 1. Chest (A) and abdominal (B and C) computerized tomographic (CT) images showing pleural and peritoneal thickening, respectively. Note the massive ascites (C).

Immunohistochemical staining

Immunohistochemical staining was performed as previously reported [11]. In brief, staining was performed using an automated immunostainer (Ventana, AZ, USA). The tumor cells including that in primary splenic foci were immunohistochemically stained for various endothelial cell markers, such as CD31 (Dako, Carpenteria, CA), vascular endothelial growth factor

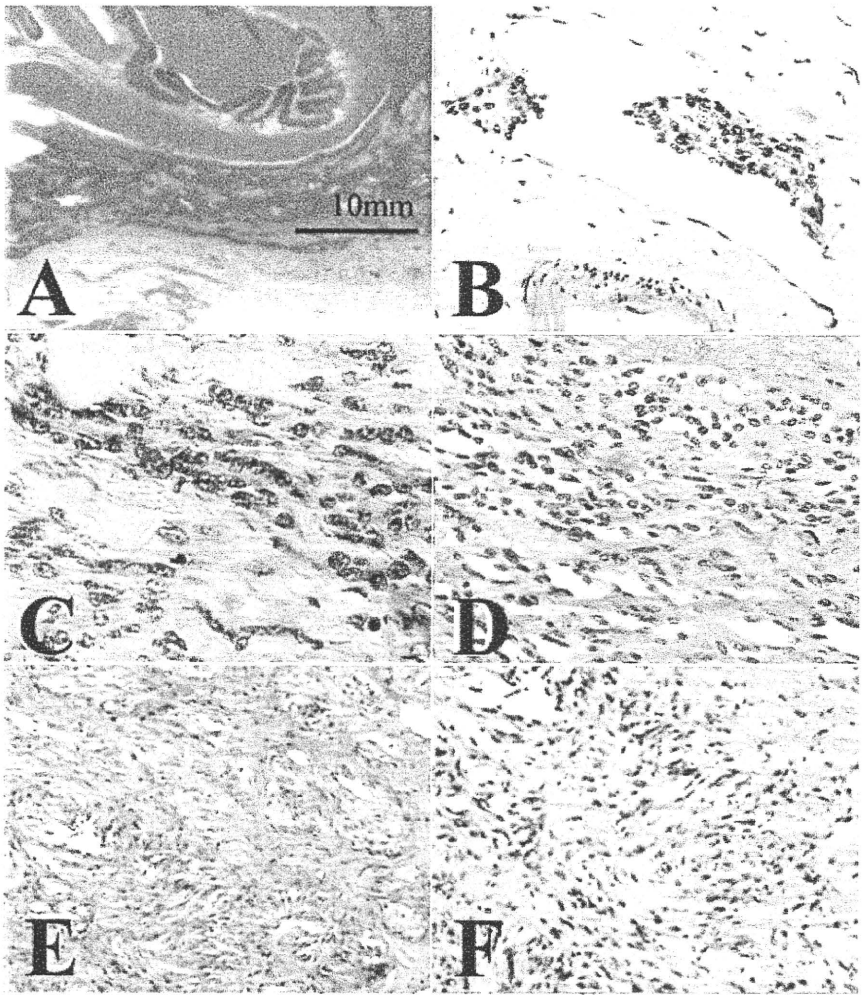

Figure 2. Visceral peritoneum was markedly thickened with dense collagenized stroma (A). Lymphatic invasion in the peritoneum is shown (B). Spindle-shaped tumor cells grew in the fibrous stroma (C). The slit-like anastomosing vascular spaces lined by the spindle-shaped tumor cells were partially observed (D). Primary splenic tumor is shown (E and F).

receptor 3 (VEGFR3) (Santa Cruz Biotechnology, Inc, Santa Cruz, CA) and podoplanin (D2-40) (DAKO). However, the tumor cells were not stained with anti-CD34 (Becton Dickinson, San Jose, CA), cytokeratin (AE1/AE3 (Boehringer-Mannheim, Indianapolis, IND,), CAM5.2 (Becton Dickinson), cytokeratin5/6 (DAKO)), S-100 (DAKO), WT-1 (Santa Cruz Biotechnology), calretinin (Novacastra, Newcastle upon Tyne, UK), or HBME-1 (DAKO). Representative result of the immunohistochemical staining is shown in Figure 3.

Malignant endothelial tumors often have an overlapping immunophenotype of vascular and lymphatic endothelial cells; therefore, the term angiosarcoma generally encompasses cases accepted as angiosarcomas and lymphangiosarcomas [12, 13]. The present tumor strongly expressed podoplanin (D2-40), which is physiologically expressed in the lymphatic endothelial cells rather than the vascular endothelial cells. Notably, the tumor cell clusters were frequently found in the non-cancerous lymphatic vessels (Figures 3B and C). In the lymphatic vessels, the line of immunoreactivity with the anti-podoplanin antibody was mostly disrupted near the tumor cell clusters.

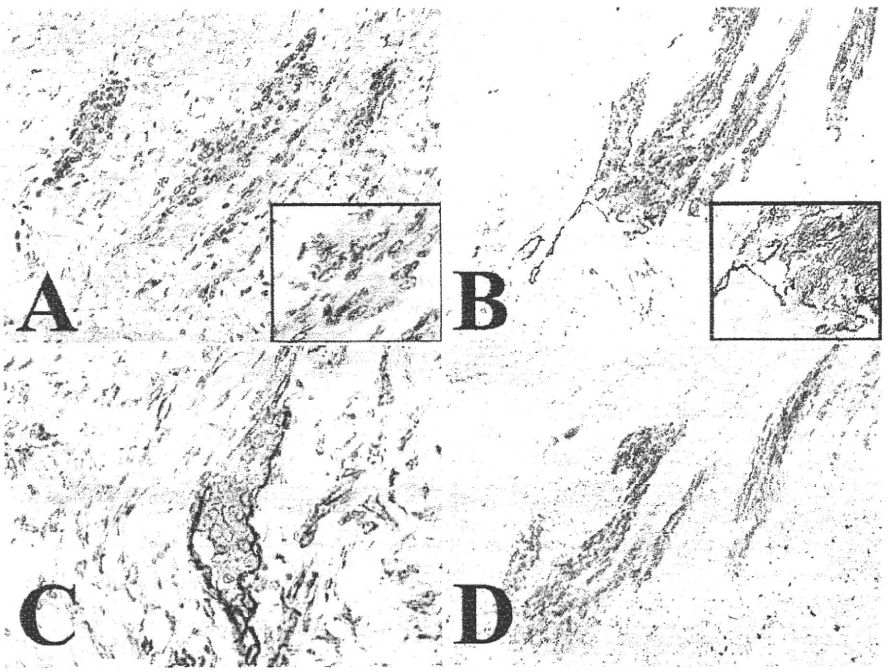

Figure 3. Representative immunohistochemical staining. Tumor cells were stained with an antibody specific to the vascular endothelial growth factor receptor 3 (VEGFR3) (A), podoplanin (B and C), and CD31 (D). Immunoreactivity with the anti-VEGFR3 antibody was observed in the cytoplasm and nuclei (A, inset). Note the tumor cell clusters in the lymphatic vessels (B and C). The walls of the affected lymphatic vessels were focally obscure; this suggested that the tumor invading to the stroma.

Taken together with the patient's clinical course, we speculate that the primary splenic angiosarcoma systemically metastasized to the peritoneum and pleura, possibly via the lymphatic route, spread to the serous membrane, and subsequently grew with the fibrous stroma in the form of a "pseudomesotheliomatous angiosarcoma."

Unique expression of MMP-1 in the angiosarcoma cells

Recent studies show that MMP-1 plays an important role in the pathogenesis of mesothelioma by degrading the interstitial collagen and remodeling the tumor stroma [8–10]. We also examined whether the tumor in the present case expressed MMP-1. As demonstrated in **Figure 4**, immunoreactivity with the antibody specific to MMP-1 (Thermo Fisher Scientific Anatomic Pathology, Fremont, CA) was found in the angiosarcoma cells of this patient (**Figure 4A** and **C**); this was similar to the immunoreactivity in the pleural mesothelioma tissues, which were stained in parallel (**Figure 4B**).

Since no report, which described the MMP-1 expression in angiosarcoma, was available, we further examined whether MMP-1 was expressed in angiosarcomas, which did not exhibit metastasis to the serous membrane. Notably, significant immunoreactivity with the anti-MMP-1 antibody was not found in any of the 7 archival pathological angiosarcoma tissue specimens.

We think that the present angiosarcoma is unique with respect to its MMP-1 expression.

Discussion

Here, we report a case of splenic angiosarcoma with a peculiar metastasis pattern, which mimics that of a mesothelioma. Pseudomesotheliomatous angiosarcoma is rare, but it has been increasingly reported in the literature or

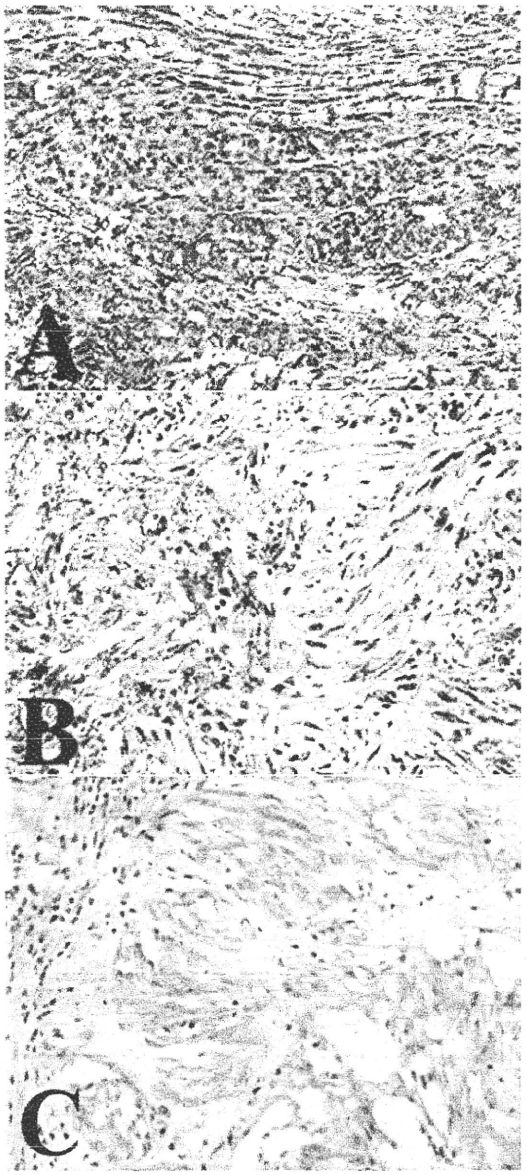

Figure 4. Representative immunohistochemical staining with the anti-MMP-1 antibody. The tumor cells in the peritoneum (A) as well as the mesothelioma tissue specimens (B) were stained with the anti-MMP-1 antibody. Notably, immunoreactivity was also found in primary splenic tumor (C).

mentioned in reference textbooks [3, 14-16]. However, the pathogenesis of pseudomesotheliomatous angiosarcoma is largely unclear. In particular, the correlation of mesothelioma and pseudomesotheliomatous angiosarcoma is an important medico-legal issue.

Some investigators have speculated that serosal angiosarcoma may represent a peculiar malignant mesothelioma differentiating along an abnormal angioblastic pathway [6]. This hypothesis is not justifiable, at least in the present case. The clinical course apparently indicated that the angiosarcoma in the present case originated in the spleen and subsequently metastasized to the serous membrane.

Pseudomesotheliomatous cancer of the lung, a well-characterized entity, is believed to be a small subpleural lung cancer that is widely disseminated via the subpleural lymphatic vessels. In the present case, tumor invasion in the lymphatic vessels was frequently found in the serous membrane (**Figures 2B**, **3B**, and **3C**). The tumor may have widely disseminated through the lymphatic route and may have invaded the serous membrane causing the remodeling of the fibrous stroma.

To elucidate the molecular mechanism underlying the generation of marked fibrous stroma, we examined MMP-1 expression in the angiosarcoma. Invasion and construction of the stroma of malignant tumor cells requires the destruction of the basement membrane and proteolysis of the extracellular matrix. MMP-1 is the only enzyme able to initiate the breakdown of the interstitial collagens, such as collagen type 1, collagen type 2, and collagen type 3 [18]. MMP-1 expression is also linked to the invasiveness of the mesothelioma cells [8-10]. As shown in Figure 4, the angiosarcoma cells in the present case expressed MMP-1 that is expressed by mesotheliomas and not by other angiosarcomas. We speculate that pseudomesotheliomatous angiosarcoma may be an angiosarcoma that has strong dissemination capability and invades the serous membrane like pseudomesotheliomatous cancer in the lung.

Acknowledgement

This work was supported by grants from the Ministry of Education of Japan (KAKEN 21590371), the Head of Kochi Medical School Hospital's Discretionary Grant, and the Medical Research Fund of Kochi Medical School.

Please address correspondence to: Tamotsu Takeuchi, MD, Department of Pathology, Kochi Medical School, Nankoku, Kochi 783-8505, Japan.

Tel: +81-88-880-2331, E-mail: takeutit08@gmail.com

References

[1] Maddox JC and Evans HL. Angiosarcoma of skin and soft tissue: a study of forty-four cases. Cancer. 1981;48:1907-1921.

[2] Falk S, Krishnan J, Meis JM. Primary angiosarcoma of the spleen: A clinicopathologic study of 40 cases. Am J Surg Pathol. 1995;19:119-120.

[3] McCaughey WT, Dardick I, and Barr JR. Angiosarcoma of serous membranes. Arch Pathol Lab Med. 1983;107:304-307.

[4] Lin BT, Colby T, Gown AM, Hammar SP, Mertens RB, Churg A, and Battifora H. Malignant vascular tumors of the serous membranes mimicking mesothelioma. A report of 14 cases. Am J Surg Pathol. 1996;20:1431-1439.

[5] Falconieri G, Bussani R, Mirra M, and Zanella M. Pseudomesotheliomatous angiosarcoma: a pleuropulmonary lesion simulating malignant pleural mesothelioma. Histopathology. 1997; 30:419-424.

[6] Hoeller H, Schmidt P, TscheliessniggKH. Malignes angioblastisches mesothelioma des Perikards. Zbl Allg. Pathol. Anat. 1979; 123:344-350

[7] Terada T, Nakanuma Y, Matsubara T, and Suematsu T. An autopsy case of primary angiosarcoma of the pericardium mimicking malignant mesothelioma. Acta Path Jpn 1988; 38: 1345-1351

[8] Harvey P, Clark IM, Jaurand MC, Warn RM, and Edwards DR. Hepatocyte growth factor/scatter factor enhances the invasion of mesothelioma cell lines and the expression of matrix metalloproteinases. Br J Cancer 2000; 83:1147-1153

[9] Liu Z, Ivanoff A, and Klominek J. Expression and activity of matrix metalloproteases in human malignant mesothelioma cell lines. Int J Cancer. 2001;91:638-643.

[10] Kroczynska B, Cutrone R, Bocchetta M, Yang H, Elmishad AG, Vacek P, Ramos-Nino M, Mossman BT, Pass HI, and Carbone M. Crocidolite asbestos and SV40 are cocarcinogens in human mesothelial cells and in causing mesothelioma in hamsters. Proc Natl Acad Sci USA. 2006;103:14128-14133.

[11] Takeuchi T, Misaki A, Liang SB, Tachibana A, Hayashi N, Sonobe H, Ohtsuki Y. Expression of T-cadherin (CDH13, H-Cadherin) in human brain and its characteristics as a negative growth regulator of epidermal growth factor in neuroblastoma cells. J Neurochem. 2000;74:1489-1497.

[12] Enzinger FM, and Weiss SW. Malignant vascular tumors. In: Enzinger FM, Weiss SW, editors. Soft tissue tumors. 3rd ed. New York: Mosby; 1994. p. 641-655.

[13] Kindblom LG, Stenman G, and Angervall L. Morphological and cytogenetic studies of angiosarcoma in Stewart-Treves syndrome. Virchows Arch A Pathol Anat Histopathol 1991; 419: 439-445.

[14] Yousem, S.A., Hochholzer, L. Unusual thoracic manifestations of epithelioid hemangioendothelioma Archives of Pathology and Laboratory Medicine. 1987; 111: 459-463.

[15] Battifora, H. Epithelioid hemangioendothelioma imitating mesothelioma. Appl. Immunohistochem. 1993; 1: 220-222.

[16] Rosai, J. Ackerman's Surgical Pathology. St Louis: Mosby 1995

[17] Harwood TR, Gracey DR, and Yokoo H. Pseudomesotheliomatous carcinoma of the lung. A variant of peripheral lung cancer. Am J Clin Pathol. 1976;65:159-167.

[18] Saffarian S, Collier IE, Marmer BL, Elson EL, and Goldberg G. Interstitial collagenase is a Brownian ratchet driven by proteolysis of collagen. Science. 2004;306:108-111.

HUMAN MUTATION Mutation in Brief #1029, 29:E271–E277, (2008) Online

MUTATION IN BRIEF

Mutations in the Small Heterodimer Partner Gene Increase Morbidity Risk in Japanese Type 2 Diabetes Patients

Mayumi Enya[1§], Yukio Horikawa[1,2§*], Eiji Kuroda[1], Kayoko Yonemaru[1], Naoko Tonooka[2], Hideaki Tomura[2], Naohisa Oda[3], Norihide Yokoi[4], Kazuya Yamagata[5†], Nobuyuki Shihara[2], Katsumi Iizuka[2], Toshiji Saibara[6], Susumu Seino[4], and Jun Takeda[1]

From the [1]Department of Diabetes and Endocrinology Division of Molecule and Structure Gifu University School of Medicine, Gifu; the [2]Laboratory of Medical Genomics, Biosignal Genome Resource Center, Institute for Molecular and Cellular Regulation, Gunma University, Maebashi; the [3]Department of Internal Medicine, Fujita Health University School of Medicine, Aichi; the [4]Department of Physiology and Cell Biology, Kobe University Graduate School of Medicine, Kobe; the [5]Department of Metabolic Medicine, Graduate School of Medicine, Osaka University, Osaka, the [6]Department of Gastroenterology and Hepatology, Kochi Medical School, Nankoku, Japan

† present affiliation: *Department of Medical Biochemistry, Faculty of Medical and Pharmaceutical Sciences, Kumamoto University*

§ These authors equally contributed to this work

*Correspondence to; Yukio Horikawa, MD, PhD
Department of Diabetes and Endocrinology, Division of Molecule and Structure, Gifu University School of Medicine, Gifu
TEL: +81-58-230-6564, FAX: +81-58-230-6376, E-mail: yhorikaw@gifu-u.ac.jp

Contract grant sponsor: This work was supported by a Health and Labor Science Research Grant for research on Human Genome and Tissue Engineering from the Japanese Ministry of Health, Labor and Welfare, a Grant-in-Aid for Scientific Research from the Japanese Ministry of Science, Education, Sports, Culture and Technology, and a New Energy and Industrial Technology Development Organization Grant.

Communicated by Michael Dean

Mutations in the small heterodimer partner gene (NR0B2; alias SHP) are associated with high birth weight and mild obesity in Japanese children. *SHP* mutations may also be associated with later obesity and insulin resistance syndrome that induces diabetes. To investigate this possibility, the prevalence of *SHP* mutations in Japanese with and without type 2 diabetes mellitus and the functional properties of the mutant proteins were evaluated. Direct sequencing of two exons and flanking sequences of *SHP* in 805 diabetic patients and 752 non-diabetic controls identified 15 different mutations in 44 subjects, including 6 novel mutations. Functional analyses of the mutant proteins revealed significantly reduced activity of nine of the mutations. Mutations with reduced activity were found in 19 patients (2.4%) in the diabetic group and in 6 subjects (0.8%) in the control group. The frequency difference between DM and control subjects adjusted for sex and age was statistically significant (P=0.029, odds ratio 2.67, 95% CI 1.05 – 6.81, 1-β=0.91). We conclude that *SHP* mutations associated with mild obesity in childhood increase susceptibility to type 2 diabetes in later life in Japanese. © 2008 Wiley-Liss, Inc.

KEY WORDS: SHP, type 2 diabetes, obesity, fatty liver, NASH

Received 16 April 2008; accepted revised manuscript 20 June 2008.

DOI: 10.1002/humu.20865

INTRODUCTION

Type 2 diabetes mellitus is characterized by defects of insulin secretion in pancreatic b-cells and insulin action in peripheral tissues. Failure of pancreatic β-cells to compensate for insulin resistance by increasing insulin secretion is thought to underlie the development of type 2 diabetes (Reaven, 1988, Polonsky, 2000).

We have previously shown that mutations in the gene encoding small heterodimer partner (*NR0B2*, alias *SHP*; MIM# 604630), an orphan nuclear receptor that interacts with a number of other receptors (Seol et al., 1996, Masuda et al., 1997, Seol et al., 1998, Johansson et al., 1999), are associated with high birth weight and mild obesity in Japanese children, although the molecular mechanisms by which the *SHP* mutations cause these disorders are unknown (Nishigori et al., 2001).

Nuclear receptors such as SHP and peroxisome proliferator-activated receptor (PPAR) α that regulate lipid metabolism in liver are potential contributors to fatty liver. It should be noted that the storage of lipids in liver can trigger inter-organ crosstalk systems that affect insulin sensitivity in muscle. Farnesoid X receptor (FXR)-null mice, with reduced levels of SHP, develop severe fatty liver and elevated circulating FFAs, which is associated with elevated serum glucose and impaired glucose and insulin tolerance resulting from attenuated inhibition of hepatic glucose production by insulin and reduced peripheral glucose disposal (Ma et al., 2006). Some patients with *SHP* mutations exhibit liver dysfunction due to fatty liver (Nishigori et al., 2001). Accordingly, mutations in *SHP* may be associated with insulin resistance due to both later obesity and also to fatty liver in Japanese subjects.

Nonalcoholic fatty liver disease (NAFLD) is a polygenic disease caused by a combination of environmental and genetic factors. Potential candidate genes contributing to NAFLD, a condition comprising a spectrum of pathological liver conditions ranging from steatosis alone to non-alcoholic steatohepatitis (NASH), include those involved in fat deposition, insulin sensitivity, and hepatic lipid oxidation, synthesis, storage, and export. NASH is believed to be a hepatic expression of metabolic syndrome (Ono and Saibara, 2006). In this regard, genetic abnormalities manifested in obesity and fatty liver might well act in concert to induce diabetes.

To evaluate the influence of *SHP* mutations on risk of later development of type 2 diabetes, we examined the frequencies of these mutations in Japanese subjects with and without type 2 diabetes mellitus as well as in patients with NASH.

MATERIALS AND METHODS

Patient populations

The ADA definitions of type 2 diabetes were used. Obesity is defined in these studies as BMI of >25 kg/m^2, in accord with the criteria of the Japan Society for the Study of Obesity (Japanese Society for the Study of Obesity, 2000) and the report by WHO (Western Pacific Region) and IASO/IOTF (International Association for the Study of Obesity/International Obesity Task Force) (WHO and IASO/IOTF, 2000). We evaluated the prevalence of SHP mutations in 805 Japanese patients with type 2 diabetes (male/female, 432/373: age, 60.3±11.8 yr.; BMI, 24.1± 4.0 kg/m^2) and 752 non-diabetic controls (male/female, 418/334; age, 59.7±13.3 yr.; BMI, 22.9±2.9 kg/m^2). Informed consent was obtained from all of the diabetic subjects and volunteer controls. NASH patients with nonalcoholic fatty liver disease underwent liver biopsy after signed informed consent and thorough clinical evaluation. Liver biopsy was analyzed by a pathologist (H.E.) and the diagnosis of NASH was based on Brunt's criteria (Brunt et al., 1999). Laboratory blood tests and BMI were analyzed in 93 biopsy-proved NASH patients (48 males and 45 females, age: 29.2 ± 5.4 years old, BMI: 29.2 ± 5.4 kg/m2, ALT: 102.6 ± 66.6 IU/L, T Chol: 5.25 ± 1.05 mmol/L, TG: 1.74 ± 0.88 mmol/L, HDL-C: 1.24 ± 0.35 mmol/L, HbA1c: 5.6 ± 1.0 %, FPG: 6.03 ± 1.79 mmol/L).

Mutation analysis

The two exons and flanking regions of the SHP gene were screened for mutations by direct DNA sequencing of the amplified polymerase chain reaction (PCR) products, using specific primer pairs and an ABI PRISM BigDye Terminator Cycle Sequencing FS ready Reaction Kit (Applied Biosystems, Foster City, CA). Primer pairs and PCR conditions used for screening of the SHP gene are as follows. Exon1: 5'-CATGACTTCTGGAGTCAAGG-3' and 5'-GTCCCTTTCAGGCAGGCATA-3',

5'-CATCCTTCTGGCAGCTGCCT-3' and 5'-TTAGAAGCTACCTTCCCTGGCT

GG-3' Exon2: 5'-CAGATCTTGGGCCAGTCTTG-3' and 5'-CTCCAGGAGCATTG GGTCAC-3'. Genomic DNA extracted from diabetic and control subjects was initially denatured at 95° C for 1 min, followed by 35 cycles of denaturation at 94° C for 30 sec, annealing at 60° C or 62° C for 30 sec, extension at 72° C for 30 sec, and a final extension step of 7 min. The sequencing reactions were analyzed by automatic DNA sequencers (Applied Biosystems models 3100 and 3700).

Mutation Nomenclature

The cDNA NM_021969.1 and protein NP_068804.1 sequences were used for mutation nomenclature, with DNA +1 corresponding to the A of the ATG translation initiation codon. Descriptions of all sequence variants were checked using the Mutalyzer program (http://www.LOVD.nl/mutalyzer/).

Functional analysis of SHP mutant proteins

Analysis of the functional properties of mutant and wild-type proteins was performed as described previously (Nishigori et al., 2001). Briefly, the *SHP* mutations newly identified in this study were generated by PCR-based site-directed mutagenesis and cloned in the expression pCMV-6b vector. The sequences for wild-type and mutant SHP proteins, and HNF-4α were cloned in pCMV-6b and pcDNA3.1 (Invitrogen, Groningen, The Netherlands), respectively. For luciferase reporter assays, the promoter region of the human HNF-1α gene was inserted into the pGL3-Basic Reporter vector (Promega, Madison, WI).

HepG2 cells ($1x10^5$) were grown in 6-well plates containing Dulbecco's modified Eagle's medium (DMEM) supplemented with 15% fetal calf serum. The cells were transfected with ExGen 500 solution (6.6 ml) (Fermentas, Ontario, Canada), 333 ng of HNF-1α-promoter/reporter construct, 100 ng of HNF-4α-expression plasmid, 0-125 ng of test DNA, and 17 ng of pRL (Renilla luciferase)-TK. Luciferase reporter activity was measured using a Dual-Luciferase Reporter Assay System (Promega) according to the manufacturer's instructions. Renilla luciferase activity was used to normalize transfection efficiencies among experiments.

Statistical analyses

Statistical difference in frequencies of *SHP* mutations between the diabetic and control groups was analyzed by logistic regression analysis, using a package of STATVIEW 5.0 (SAS Institute Inc., Cary, NC). Data obtained by luciferase reporter assay were analyzed by the Student's *t*-test.

RESULTS

Eight hundred five Japanese patients with adult-onset type 2 diabetes (T2DM), 752 non-diabetic controls, and 93 patients with NASH were examined. Screening of the SHP gene (*NR0B2*) by direct sequencing resulted in the identification of fifteen different mutations (c.100C>T [p.Arg34X], c.112C>T [p.Arg38Cys], c.134G>C [p.Arg45Pro], c.157_166del [p.His53AlafsX50], c.160C>T [p.Arg54Cys], c.169C>T [p.Arg57Trp], c.292_300delinsAC [p.Leu98ThyfsX6], c.314T>G [p.Val105Gly], c.512G>C [p.Gly171Ala], c.532G>A [p.Asp178Asn], c.566G>A [p.Gly189Glu], c.583G>T [p.Ala195Ser], c.618G>A [p.Trp206X], c.637C>T [p.Arg213Cys], and c.647G>A [p.Arg216His]) including six novel mutations in type 2 diabetic patients (Table 1),

eight of which were previously identified in obese children (Nishigori et al., 2001) and one of which, p.Gly171Ala, was reported as a polymorphism in a study of Caucasians (Hung et al., 2003, Echwald et al., 2004, Mitchell et al., 2003). In NASH patients, only one mutation, p.Arg45Pro, was identified. We could not find any variants in flanking sequences.

Table 1: Mutations identified in the human SHP gene (*NR0B2*).

Exon	Codon	Nucleotide change	Designation	Patients (n=805)	Controls (n=752)
Mutations with reduced activity					
1	34	c.100C>T	p.Arg34X [a)b)c)d)e)]	2	0
1	53	c.157_166del	p.His53AlafsX50 [a)b)c)e)]	2	0
1	54	c.160C>T	p.Arg54Cys*	0	1
1	57	c.169C>T	p.Arg57Trp [a)]	1	0
1	98	c.292_300 delinsAC	p.Leu98ThyfsX6 [a)c)e)]	6	1
1	105	c.314T>G	p.Val105Gly*	1	0
2	189	c.566G>A	p.Gly189Glu [a)]	3	0
2	195	c.583G>T	p.Ala195Ser [a)c)d)e)]	1	3
2	206	c.618G>A	p.Trp206X*	2	1
2	213	c.637C>T	p.Arg213Cys [a)b)c)e)]	1	0
			sum	19 (2.4%)	6 (0.8%)
Mutations with normal activity					
1	38	c.112C>T	p.Arg38Cys*	1	0
1	45	c.134G>C	p.Arg45Pro*	1	0
1	171	c.512G>C	p.Gly171Ala	0	1
1-2	178	c.532G>A	p.Asp178Asn*	1	0
2	216	c.647G>A	p.Arg216His	6	9
			sum	9 (1.1%)	10 (1.3%)

* indicates six novel variants identified in the present study.

To determine if the mutations alter the function of the SHP protein, the effect of the wild-type and mutant proteins on HNF-4α-mediated transactivation of HNF-1α gene transcription in HepG2 cells was examined by luciferase reporter assay (Fig. 1 and Nishigori et al., 2001). a) early-onset obesity, b) high birth weight, c) diabetes, d) fatty liver, e) decreased insulin sensitivity (Nishigori et al., 2001) Mutations were numbered according to GenBank NM_021969.1 and NP_068804.1. Nucleotide +1 is A of the ATG initiation codon.

Functional analyses of the novel mutant proteins showed significantly reduced activity of transcriptional regulation of HNF-4α, except in the case of p.Arg38Cys, p.Arg45Pro, and p.Asp178Asn. The results of functional analyses of the mutations newly identified in this study are shown in Fig. 1. The mutations with reduced activity were found in nineteen subjects (2.4%) in the diabetic group, six (0.8%) in the control group, and none in the NASH group (Table 1). The frequency difference between DM and control groups was statistically significant by logistic regression analysis considering gender and age (P=0.029; 1-β =0.91) with odds ratio of 2.67 [95% CI, 1.05-6.81]. This frequency difference between DM and control groups came to be not statistically significant by logistic regression analysis when considering gender, age, and BMI (P=0.078), with odds ratio of 2.26 [95% CI, 0.87-5.86]. Furthermore, subjects with mutations of reduced activity showed significantly higher BMI than subjects without the mutations (25.6±4.6 vs 23.5±3.6, P=0.0039 in combined subjects, and 24.0 ± 4.0 vs. 26.5 ± 5.0, P=0.012 in diabetic patients). In control subjects, those with mutations of reduced activity showed similar BMI to those without mutations (22.9 ± 2.9 vs. 23.1 ± 2.7, P=0.87).

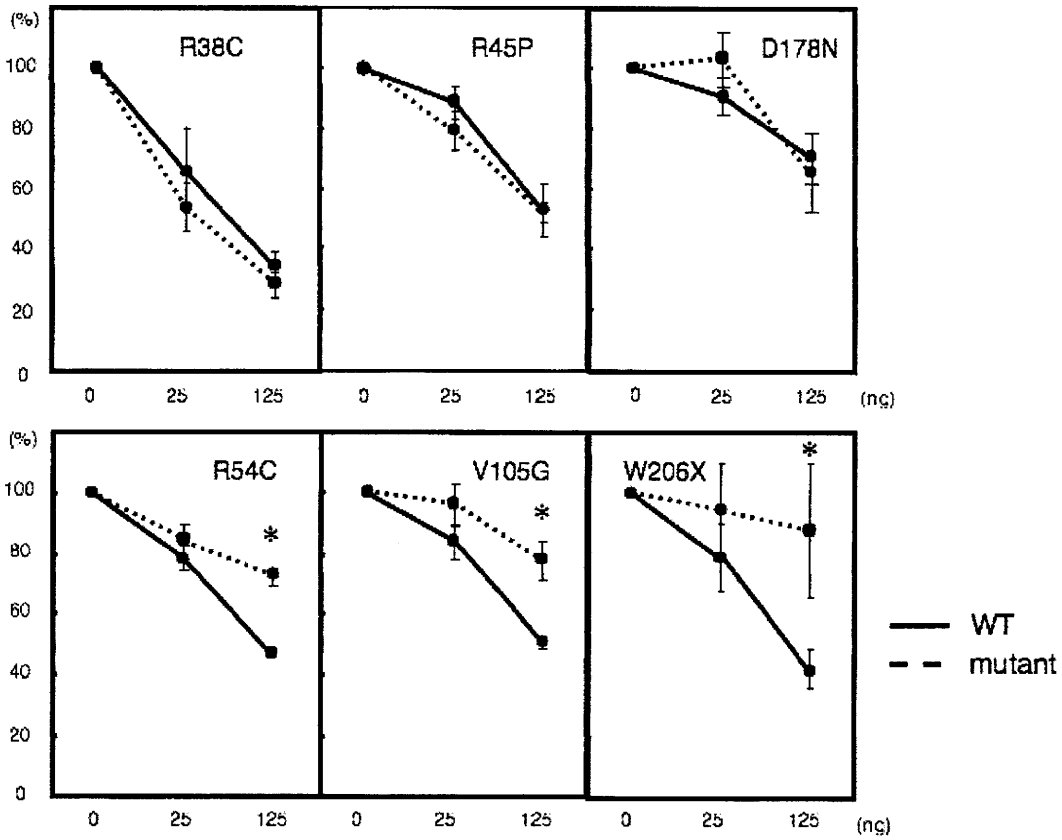

Figure 1: Inhibition of transactivation activity of HNF-4α by wild-type and mutant SHP proteins. It has been shown previously that expression of wild-type SHP significantly decreases HNF-4α transactivation of the HNF-1α gene prompter in HepG2 cells, indicating that SHP is a negative regulator of HNF-4α (Nishigori et al., 2001, Lee et al., 2000). Transcriptional regulation of the novel six mutations of p.Arg38Cys, p.Arg45Pro, p.Arg54Cys, p.Val105Gly, p.Asp178Asn and p.Trp206X was exaimined by luciferase reporter assay (n=3 in each experiment). Functional properties of the other mutations identified have been examined previously (Nishigori et al., 2001, Echwald et al., 2004). The relative luciferase activity (firefly/Renilla) of each construct at 0 ng, 25 ng, and 125 ng of wild-type and mutant SHP proteins was measured in HepG2 cells. Percent activity in relation to basic HNF-4 α activity is shown as mean ± SD. * $P<0.05$.

DISCUSSION

Mutations in the SHP gene have been shown to be associated with high birth weight and early-onset mild obesity in Japanese. Although the molecular mechanism by which these mutations increase body weight is unknown at present, one possibility is suggested by the fact that pancreatic β cells express SHP mRNAs at high levels. Since SHP inhibits HNF-4α (MODY1 protein) (Nishigori et al., 2001,Lee et al., 2000), functional defects of SHP might well increase the activity of HNF-4α and other downstream components of glycolytic signal transduction (Dukes et al., 1998), resulting in increased insulin secretory response to glucose (Wang et al., 2006). In addition, since insulin is a key hormone in fetal growth, high levels of fetal insulin may well be associated with high birth weight and postnatal obesity.

As adult-onset type 2 diabetes is a polygenic disorder requiring interaction of multiple genetic and environmental factors, and Japanese patients exhibit a lesser insulin secretory capacity due to pancreatic β–cell

dysfunction (Kosaka et al., 1977, Kosaka and Akanuma, 1980, Yoshinaga and Kosaka, 1999), the increased insulin secretory demand associated with *SHP* mutations might increase susceptibility to type 2 diabetes in this population. Since other nuclear receptors that interact with SHP in peripheral tissues (Seol et al., 1996, Masuda et al., 1997, Seol et al., 1998, Johansson et al., 1999) may be involved in the pathogenesis of insulin resistance due to obesity or fatty liver, the secondary demand for compensatory insulin secretion might also promote the development of overt diabetes.

FXR-null mice, which show reduced levels of SHP, exhibit elevated plasma cholesterol and triglyceride levels and excessive accumulation of fat in the liver (Ma et al., 2006). Fatty liver also was observed in some early-onset obesity patients with *SHP* mutations (Nishigori et al., 2001). In addition, increased insulin secretion derived from *SHP* mutations accelerates fat accumulation in the liver. Accordingly, we examined 93 NASH patients, and found one mutation. However, none of the mutations associated with reduced activity was found in the NASH group, suggesting that the effect of SHP on the accumulation of fat in the liver may be of little clinical importance.

While we cannot link the etiology of NASH to mutation of *SHP*, the finding that *SHP* mutations increase morbidity risk for type 2 diabetes due to mild obesity in later life in Japanese suggests a genetic link between obesity and type 2 diabetes in human. To clarify the complex relationship of type 2 diabetes with SHP deficiency, further genetic analysis and characterization of the diabetogenic factors involved is required.

According to previous epidemiological studies, low birth weight and fetal thinness are associated with insulin resistance syndrome and were therefore thought to be related to later risk of type 2 diabetes (Hales et al., 1991, Eriksson et al., 2003). In contrast, we demonstrate here an increased morbidity risk of type 2 diabetes due to *SHP* mutations associated with high birth weight and mild obesity in Japanese children. Further analysis of the functional properties of mutant SHP proteins in energy expenditure should provide new insight into the relationship between birth weight and the development of type 2 diabetes.

ACKNOWLEDGMENTS

We thank Tsuchida H., Yokoyama K., Uda I., and Ibe Y. for technical assistance.

REFERENCES

Brunt EM, Janney CG, Di Bisceglie AM, Neuschwander-Tetri BA, Bacon BR. 1999. Nonalcoholic steatohepatitis: a proposal for grading and staging the histological lesions. Am J Gastroenterol 94: 2467-2474

Dukes ID, Sreenan S, Roe MW, Levisetti M, Zhou YP, Ostrega D, Bell GI, Pontoglio M, Yaniv M, Philipson L, Polonsky KS. 1998. Defective pancreatic b-cell glycolytic signaling in hepatocyte nuclear factor-1α-deficient mice. J Biol Chem 273: 24457-24464

Echwald SM, Andersen KL, Sorensen TIA, Larsen LH, Andersen T, Tonooka N, Tomura H, Takeda J, Pedersen O. 2004. Mutation analysis of NR0B2 among 1545 Danish men identifies a novel c. 278 G>A (p. G93D) variant with reduced functional activity. Hum Mutat 24: 381-387

Eriksson JG, Forsen T, Tuomilehto J, Osmond C, Barker DJP. 2003. Early adiposity rebound in childhood and risk of type 2 diabetes in adult life. Diabetologia 46: 190-194

Hales CN, Barker DJP, Clark PMS, Cox LJ, Fall C, Osmond C, Winter PD. 1991. Fetal and infant growth and impaired glucose tolerance at age 64. BMJ 303: 1019-1022

Hung CC, Farooqi IS, Ong K, Luan J, Keogh JM, Pembrey M, Teo GSH, Dunger D, Wareham NJ, O'Rahilly S. 2003. The contribution of variants in the small heterodimer partner gene to birthweight, adiposity and insulin levels: Mutational analysis and association studies in multiple populations. Diabetes 52:1288-1291

Japanese Society for the Study of Obesity. 2000. Committee Report. J Jpn Soc Study Obes 6: 18-28

Johansson L, Thomsen JS, Damdimopoulos AE, Spyrou G, Gustafsson J-A, Treuter E. 1999. The orphan nuclear receptor SHP inhibits agonist-dependent transcriptional activity of estrogen receptors ERα and ERβ. J Biol Chem 274: 345-353

Kosaka K, Hagura R, Kuzuya T. 1977. Insulin responses in equivocal and definite diabetes, with special reference to subjects who had mild glucose intolerance but later developed definite diabetes. Diabetes 26: 944-952

Kosaka K, Akanuma Y. 1980. Heterogeneity of plasma IRI responses in patients with IGT. Diabetologia 18: 347-348

Lee Y-K, Dell H, Dowhan DH, Hadzopoulou-Cladaras M, Moore DD. 2000. The orphan nuclear receptor SHP inhibits hepatocyte nuclear factor 4 and retinoid X receptor transactivation: Two mechanisms for repression. Mol Cell Biol 20: 187-195

Ma K, Saha PK, Chan L, Moore DD. 2006. Farnesoid X receptor is essential for normal glucose homeostasis. J Clin Invest 116: 1102-1109

Masuda N, Yasuno H, Tamura T, Hashiguchi N, Furusawa T, Tsukamoto T, Sadano H, Osumi T. 1997. An orphan nuclear receptor lacking a zinc-finger DNA-binding domain: interaction with several nuclear receptors. Biochim Biophys Acta 1350: 27-32

Mitchell SM, Weedon MN, Owen KR, Shields B, Wilkins-Wall B, Walker M, McCarthy MI, Frayling TM, Hattersley AT. 2003. Genetic variation in the small heterodimer partner gene and young-onset type 2 diabetes, obesity, and birth weight in U.K. subjects. Diabetes 52: 1276-1279

Nishigori H, Tomura H, Tonooka N, Kanamori M, Yamada S, Sho K, Inoue I, Kikuchi N, Onigata K, Kojima I, Kohama T, Yamagata K, Yang Q, Matsuzawa Y, Miki T, Seino S, Kim M-Y, Choi H-S, Lee Y-K, Moore DD, Takeda J. 2001. Mutations in the small heterodimer partner gene are associated with mild obesity in Japanese subjects. Proc Natl Acad Sci USA 98: 575-580

Ono M, Saibara T. 2006. Clinical features of nonalcoholic steatohepatitis in Japan: evidence from the literature. J Gastroenterol 41: 725-732

Polonsky KS. 2000. Dynamics of insulin secretion in obesity and diabetes. Int J Obes Relat Metab Disord (Suppl.) 2: S29-31

Reaven GM. 1988. Role of insulin resistance in human disease. Diabetes 37: 1595-1607

Seol W, Choi H-S, Moore DD. 1996. An orphan nuclear hormone receptor that lacks a DNA binding domain and heterodimerizes with other receptors. Science 272: 1336-1339

Seol W, Hanstein B, Brown M, Moore DD. 1998. Inhibition of Estrogen receptor action by the orphan receptor SHP (short heterodimer partner). Mol Endo 12: 1551-1557

Wang L, Huang J, Saha P, Kulkarni RN, Hu M, Kim YD, Park KG, Chan L, Rajan A, Lee I, Moore DD. 2006. Orphan receptor SHP is an important mediator of glucose homeostasis. Mol Endocrinol 20: 2671-81

WHO (Western Pacific Region) and IASO (The International Association for the Study of Obesity) /IOTF (The International Obesity Task Force). 2000. The Asia-Pacific perspective: Redefining obesity and its treatment. Web site URL; http://www.diabetes.com.au/pdf/obesity_report.pdf

Yoshinaga H, Kosaka K .1999. Heterogeneous relationship of early insulin response and fasting insulin level with development of non-insulin-dependent diabetes mellitus in non-diabetic Japanese subjects with or without obesity. Diabetes Res Clin Pract 44: 129-136

Preserved tissue structure of efferent ductules in aromatase-deficient mice

Katsumi Toda[1], Teruhiko Okada[2], Yoshihiro Hayashi[3] and **Toshiji Saibara[4]**

Departments of [1]Biochemistry, [2]Anatomy and Cell Biology, [3]Pathology and [4]Gastroenterology and Hepatology, School of Medicine, Kochi University, Nankoku, Kochi 783-8505, Japan

(Correspondence should be addressed to K Toda; Email: todak@kochi-u.ac.jp)

Abstract

Estrogen receptor α (*Esr1*) is proposed to play a critical role in the regulation of testicular fluid reabsorption at efferent ductules, and disruption of the *Esr1* gene ($Esr1^{-/-}$) resulted in marked dilation of the lumens of efferent ductules. This study was aimed to clarify whether disruption of the gene for aromatase (*Ar*), an enzyme responsible for estrogen biosynthesis, results in morphological and transcriptional alterations at efferent ductules as observed in $Esr1^{-/-}$ mice. Histology demonstrated structural preservation of the ducts in aromatase-deficient ($Ar^{-/-}$) mice. Electron microscopic examinations reveal that endocytic apparatus and tubule-cisternal endoplasmic reticulum are present in non-ciliated cells irrespective of the genotypes. However, electron-dense and acid phosphatase-negative granules and apical tubules, which are components thought to be related to membrane recycling of endosomes, are observed only in wild-type (WT) and $Ar^{-/-}$ mice. By contrast, the Golgi complex is highly developed in $Esr1^{-/-}$ mice when compared with WT and $Ar^{-/-}$ mice. RT-PCR analysis reveals no significant differences in the expression levels of a subset of genes involved in ion transportation. Thus, from the structural and transcriptional points of view, the efferent ductules of $Ar^{-/-}$ mice are indistinguishable from those of WT mice. Moreover, data from electron microscopic examinations indicate the possible involvement of *Esr1* in the regulation of vesicle recycling processes.

Journal of Endocrinology (2008) **199,** 137–146

Introduction

Testicular development and the maintenance of spermatogenesis are controlled mainly by gonadotropins and androgens (Holdcraft & Braun 2004). However, besides the well-known negative effect of estrogens on the secretion of gonadotropins, they have been shown to directly regulate testicular functions (Simpson *et al.* 1994, Carreau *et al.* 2006, Ebling *et al.* 2006). Estrogens are synthesized by an enzyme complex, aromatase, through the conversion of androgens to estrogens in Sertoli cells in immature animals and in Leydig cells in adults (Rommerts *et al.* 1982, Simpson *et al.* 1994, O'Donnell *et al.* 2001). Furthermore, germ cells were proposed to be one of the major sites for estrogen synthesis in adult mouse testis (Nitta *et al.* 1993).

Estrogens are thought normally to modulate the transcription of specific genes in estrogen target tissues through binding to estrogen receptors of either α- or β-subtype (Couse & Korach 1999, Nilsson *et al.* 2001). Both subtypes have been reported to be expressed abundantly in the efferent ductules (Zhou *et al.* 2002), where a large part of testicular luminal fluid is reabsorbed to concentrate spermatozoa (Clulow *et al.* 1998, Hess 2000). *Esr1* gene knockout ($Esr1^{-/-}$) mice display dilation of the lumens of the efferent ductules, of which the diameter becomes more than double the size of wild-type (WT) males (Hess *et al.* 1997), indicating that luminal fluid is not removed causing accumulation of fluids in the lumen of the efferent and seminiferous tubules. As $Esr2^{-/-}$ mice did not display apparent morphological abnormalities in the efferent ductules (Krege *et al.* 1998, Antal *et al.* 2008) and the phenotype of $Esr1^{-/-}Esr2^{-/-}$ mice was similar to that of $Esr1^{-/-}$ mice (Couse *et al.* 1999), *Esr1* rather than *Esr2* plays a major role in normal fluid reabsorption at the efferent ductules. Nevertheless, the requirement of aromatase activity for *Esr1* to function at the ducts has not been established.

Because estrogens are synthesized by aromatase in the testis, aromatase gene knockout ($Ar^{-/-}$) mice are a useful animal model to assess the testicular function of estrogens *in vivo*. Three lines of $Ar^{-/-}$ mice have been generated independently (Fisher *et al.* 1998, Honda *et al.* 1998, Toda *et al.* 2001*a*). However, the testicular phenotypes are variable among the lines. The $Ar^{-/-}$ mice generated by us were nearly infertile and showed no disruptions in spermatogenesis until 10 months of age, although an apparent reduction in seminiferous epithelial height was observed at that age (Toda *et al.* 2001*b*). The $Ar^{-/-}$ males generated by other group are reportedly fertile at 12–14 weeks of age and one of four $Ar^{-/-}$ mice examined displayed grossly dysmorphic seminiferous tubules

DOI: 10.1677/JOE-08-0257
0022–0795/08/0199–137 Online version via http://www.endocrinology-journals.org

Table 1 Primer pairs used for RT-PCR

Gene	5′ Primer primer	3′ Primer primer	Size (bp)
Atp1a1	GGGGATTGTTGGCTCTGATG	TTTGTCCGTTTTGGGGTTTC	328
Cftr	CTGGAGGCGAAATGGTTGTC	TTGGTATGTTATGGGGTCTA	530
Slc9a1	GGCCAACATCTCCCACAAAT	GCCTGCTTCATCTCCATCTT	651
Slc9a3	GGATGAAAAGCAGGACAAGG	AGGGGAGAACACGGGATTAT	343
Gapdh	CGGATTTGGTCGTATTGG	TCCTGGAAGATGGTGATG	210

and disrupted spermatogenesis at 4·5 months of age (Robertson *et al.* 1999, 2001). This phenotypic heterogeneity in spermatogenesis between the $Ar^{-/-}$ lines seems to be attributable to differences in genetic backgrounds rather than in the genomic region used for the gene inactivation, as the *neo* gene was inserted at the EcoRV site in exon 9 of *Cyp19a1* for the disruption of the gene in both $Ar^{-/-}$ lines (Fisher *et al.* 1998, Toda *et al.* 2001*a*). We thus generated fully congenic $Ar^{-/-}$ mice with a C57BL/6J background by repeated backcrossing to C57BL/6J mice. This study was conducted using $Ar^{-/-}$ mice with a C57BL/6J genetic background to examine the effects of aromatase inactivation on spermatogenesis and the efferent ductules with special reference to the changes observed in the tissue sites of $Esr1^{-/-}$ mice.

Materials and Methods

Experimental animals

The animal experiments were carried out according to the Guidelines of our Institutional Animal Regulations. All animals were maintained on a 12 h light:12 h darkness cycle at 22–25 °C and given water *ad libitum* and a chow, NIH-07PLD, which was developed by the National Institute of Health (USA) in order to lower phytoestrogen contents in the chow (Oriental Yeast Co., Tokyo, Japan; Yamasaki *et al.* 2002). *Cyp19a1* was disrupted by homologous recombination (Toda *et al.* 2001*a*) and the genetic background was unified to C57BL/6J by repeated backcrossing. $Esr1^{+/-}$ mice (Lubahn *et al.* 1993) were purchased from Taconic Farms, Inc. (Hudson, NY, USA) and bred in the animal facility of Kochi University to yield $Esr1^{+/-}$ mice with a C57BL/6J genetic background. $Esr1^{-/-}$ mice were generated by crossing of $Esr1^{+/-}$ mice. Mice at 5 or 10 months of age were used for this study.

Table 2 Summary of spermatogenic phenotype of mice with the C57BL/6J genetic background. Testes of WT, $Ar^{-/-}$, and $Esr1^{-/-}$ mice at 5 or 10 months of age were histologically examined.

Age	WT	$Ar^{-/-}$	$Esr1^{-/-}$
5 M	0[a]/44[b] (0%)	13/20 (65%)	14/14 (100%)
10 M	0/8 (0%)	9/13 (69%)	ND

[a]Number of mice showing spermatogenic impairment.
[b]Number of mice examined.

Histological examination

Testes and efferent ductules were fixed in a solution of 10% (v/v) buffered formalin for 24 h, dehydrated in graded ethanol, and then embedded in paraffin. Samples were cut into 3 μm thick sections and stained with hematoxylin–eosin. The luminal areas of the efferent ductules were quantified using MacScope (ver. 2.5.9) software.

Electron microscopic examination

The efferent ductules were fixed in modified Karnovsky's fixative containing 2% paraformaldehyde, 2% glutaraldehyde, and 0·05% $CaCl_2$ in 0·1 M cacodylate buffer (pH 7·2) for 1 h at 4 °C. The specimens were post-fixed with 1% osmium tetroxide in 0·1 M cacodylate buffer (pH 7·2) containing 0·8% potassium ferrocyanide for 2 h in the dark to preserve the structure of tubule-cisternal endoplasmic reticulum (TCER; Møller *et al.* 1983). After rinsing, the specimens were exposed to en bloc stain in 1% uranyl acetate in 0·05 M sodium maleate (pH 6·0) for 1 h in the dark. After rinsing in 0·05 M sodium maleate (pH 5·0) for 1 h, the specimens were dehydrated in a graded series of alcohol (Karnovsky 1967), and embedded in Spurr's resin. Thin sections were observed using a Hitachi H-7000H electron microscope. Acid phosphatase activity was detected by means of a cerium-based cytochemical method to identify lysosomes (Robinson *et al.* 1986).

Western blot analysis

The efferent ductules were kept in RNAlater (Ambion, Austin, TX, USA) at −20 °C until use. After removing the fat and connective tissue under a microscope, the tissues were minced using scissors and homogenized in an ice-cold homogenization buffer consisting of 50 mM Tris–HCl buffer (pH 7·4), 0·4 M NaCl, 0·1 mM EDTA, 0·1 mM EGTA, and protease inhibitor cocktail (Roche). The protein concentration of the homogenate was measured with a BCA protein assay reagent (Pierce, Rockford, IL, USA). Each sample (40 μg) was subjected to SDS-PAGE in a 10% gel. The separated polypeptides were then transblotted onto a polyvinylidene difluoride (PVDF) membrane. After treatment with blocking agent, the membrane was incubated with anti-*Esr1* antibody at a dilution of 1:2000 (MC-20; Santa Cruz Biotechnology, Inc., Santa Cruz, CA, USA).

After washing, the membrane was subsequently incubated with horseradish peroxidase (HRP)–anti-rabbit antibody and the enzyme activity of HRP was detected with an ECL western blotting detection kit. After detaching the anti-*Esr1* antibody, the same membrane was reprobed with an HRP–anti-β-actin monoclonal antibody (Sigma–Aldrich, Inc). The results were quantified using Quantity One (ver. 3.0) software (PDI Inc., Huntington Station, NY, USA).

RNA preparation and RT-PCR analysis

Total RNA was extracted from pooled efferent ductules kept in RNA later as described (Zarlenga & Gamble 1987) after removing fat and connective tissue under a microscope. Total RNA (1 μg) was reversed transcribed using oligo-dT primers (Ambion) and Moloney murine leukemia virus reverse transcriptase (Invitrogen) in a total volume of 25 μl per

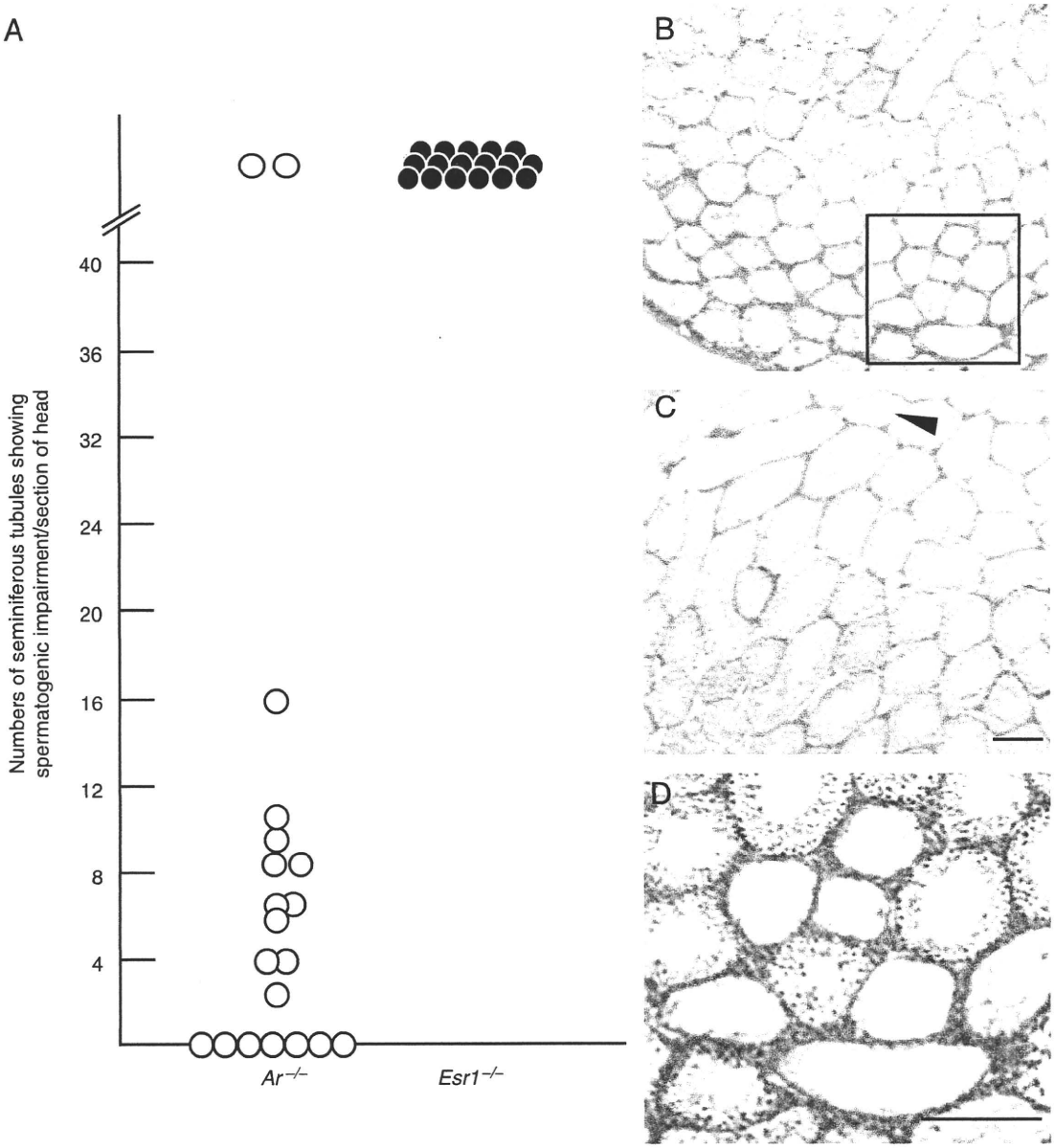

Figure 1 Histological examination of the testes of $Ar^{-/-}$ and $Esr1^{-/-}$ mice with a C57BL/6J genetic background. (A) Each circle represents an individual mouse, of which both testes were examined histologically. Vertical numerals indicate the sum of the numbers of seminiferous tubules showing impaired spermatogenesis per section in each mouse examined. As no abnormality was found in the testes of WT mice with a C57BL/6J background, the data were not plotted in this figure. (B and C) Representative photographs of the testis of an $Ar^{-/-}$ mouse at 5 months of age displaying various degrees of impairment in spermatogenesis. The seminiferous tubules indicated by arrowhead in (C) are judged to be impaired. (D) The image shown at higher magnification is from the area indicated by a box in (B). Scale bar, 200 μm.

reaction, according to the manufacturer's instructions. The expression levels of genes for ATPase, Na^+/K^+ transporting, α-1 polypeptide (*Atp1a1*), cystic fibrosis transmembrane conductance regulator homolog (*Cftr*), solute carrier family 9 (sodium/hydrogen exchanger) member 1 (*Slc9a1*), and solute carrier family 9 (sodium/hydrogen exchanger) member 3 (*Slc9a3*) were examined. PCR was carried out with 1·5 μl of the RT samples in a 30 μl reaction volume. Cycling parameters were as follows: an initial melting step of 94 °C for 1 min, amplification by 28 cycles at 94 °C for 30 s, 60 °C for 30 s, and 74 °C for 45 s and then a final 5 min at 74 °C for extension. The amplified DNA products were resolved on 5% polyacrylamide gels. After staining the gels with ethidium bromide, the banding pattern of amplified DNA fragments was recorded using a charged-coupled device camera (Sony Corp., Tokyo, Japan). The results were

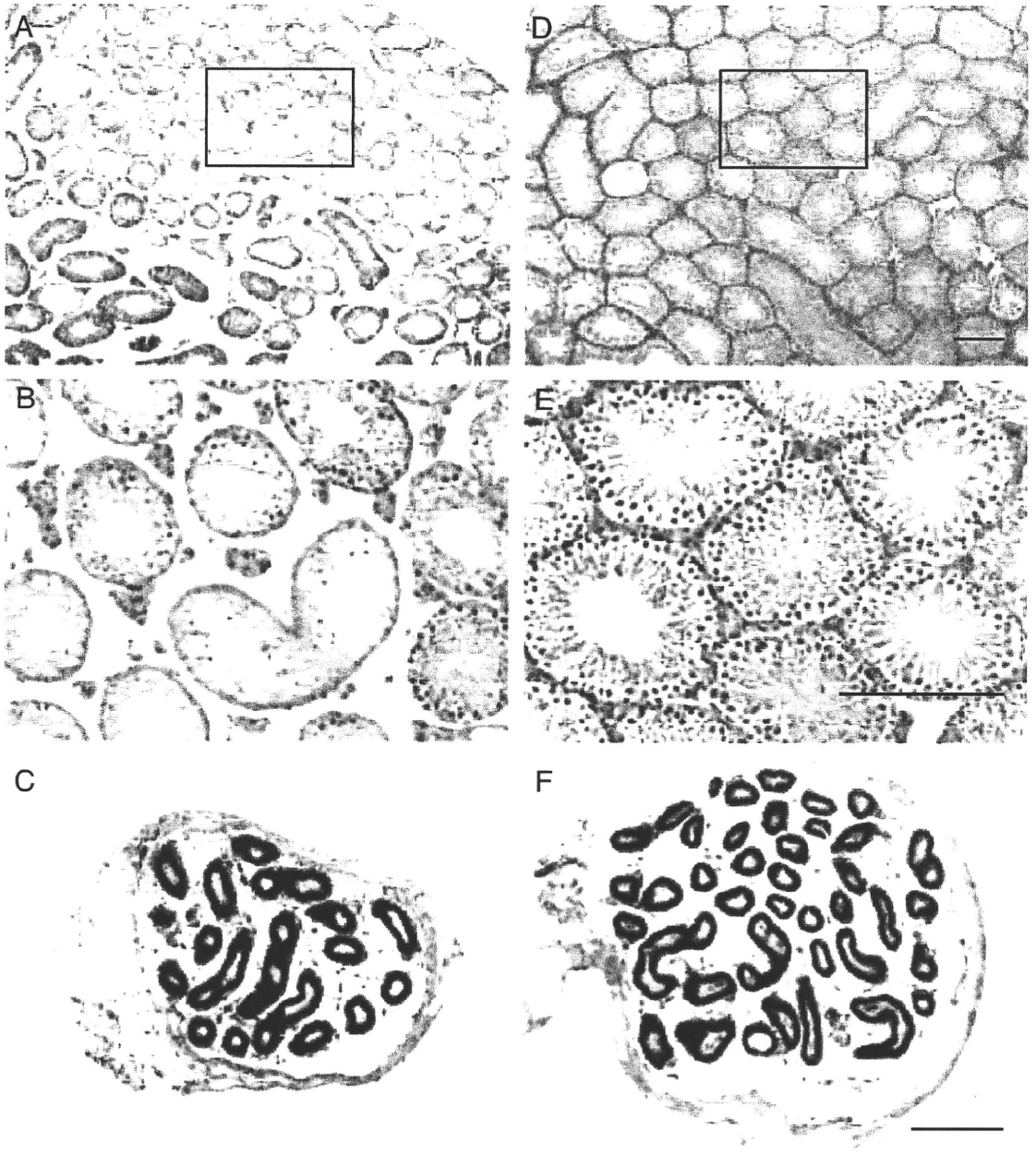

Figure 2 Photomicrographs of the testis and efferent ductules in the distal region of two individual $Ar^{-/-}$ mice at 5 months of age. (A and B) Testis from one $Ar^{-/-}$ mouse at 5 months of age showed spermatogenic impairment and (D and E) the testis from the other $Ar^{-/-}$ mouse displayed morphologically normal spermatogenesis. (B and E) The images shown at higher magnification are from the areas indicated by boxes in (A) and (D) respectively. (C and F) Both $Ar^{-/-}$ mice reveal similar morphology in the distal efferent ductules. Scale bars, 200 μm.